

# Multimodal magnetic resonance imaging in the diagnosis and therapeutical follow-up of brain tumors

Abdelkhalek Housni, PhD, Saïd Boujraf, MedSc, PhD.

## ABSTRACT

يسهم التصوير بالرنين المغناطيسي متعدد الطرق بمساهمة هامة في مجال أبحاث السرطان. فهذه التقنية هي أمانة كلياً وغير مؤينة وتوفر معلومات أساسية للتشخيص والأجوبة على الأسئلة من المعالجين قبل وأثناء وبعد العلاج. في هذه الورقة نستعرض الفائدة من طرق التصوير بالرنين المغناطيسي وتأثيراتها على التشخيص وبعد الرعاية العلاجية لمرضى أورام الدماغ. تسمح طرق التصوير بالرنين المغناطيسي بتحديد موقع عملية التوسع للأورام، والتفرقة بين أورام الدماغ والأفات المختلفة، وتشخيص نوع الورم، وتقييم وتصنيف نوع ودرجة الورم، فضلاً على المتابعة العلاجية. إن التصوير بالرنين المغناطيسي متعدد الطرق نهج له مساهمة كبيرة في مجال الرعاية المتقدمة لمرضى أورام الدماغ.

Multimodal MRI has an important contribution to cancer research. This technique is completely non-invasive and non-ionizing, it provides major information for diagnosis, and answers the questions of therapists before, during, and after treatment. Hence, in this paper we review the interest of these MRI modalities and their impact on the diagnosis, during and after therapeutic care of brain tumors. The MRI modalities allow specifying the localization of the expanding pathological tumoral process, the differential diagnosis between brain tumors and confined lesions of different categories, the diagnosis of the tumoral type of the lesion, assessing the histological grade in cases of glial tumor, and its local extension as well as the therapeutic follow-up. The multimodal MRI approach has a major contribution to the advanced care of brain tumors.

*Neurosciences 2013; Vol. 18 (1): 3-10*

*From the Department of Radiology and Medical Imaging (Housni), University Hospital of Fez, and the Department of Biophysics and Clinical MRI Methods (Boujraf), Faculty of Medicine, University of Fez, Fez, Morocco.*

*Address correspondence and reprint request to: Prof. Dr. Saïd Boujraf, Department of Biophysics and Clinical MRI Methods, Faculty of Medicine, University of Fez, BP. 1893; Km 2.200, Sidi Hrazem Road, Fez 30000, Morocco. Tél. +212 (535) 619320 Ext. 317. Fax. +212 (535) 619321. E-mail: sboujraf@gmail.com*

Protons are the most abundant nucleus biological tissues; they constitute 2/3 of material available in the human body presenting high sensitivity while interacting with static magnetic fields and magnetic field gradients.<sup>1-5</sup> The MRI represents clinical applications of these interactions, based on the detection of the hydrogen nuclei contained in water molecules very abundant in all the human tissues.<sup>1-6</sup> The MRI techniques are constantly improving.<sup>7</sup> Hence, the human body analysis reproduced in the anatomophysiological and functional study techniques contributed to the advancement of care of brain tumors. This allowed the joint supply of anatomophysiological (anatomical MRI), functional (diffusion, perfusion, bolus contrast, “BOLD”, and so forth) and metabolic information provided by magnetic resonance spectroscopy (MRS).<sup>1,2,8-22</sup> The major advantage of this imaging approach is that it is completely non-invasive.<sup>3,7,13-15</sup> The combination and confrontation of the various MRI modalities’ data supply clinicians with valuable information allowing improvement in the diagnostic approach that is decisive in many pathological situations. In this paper, we review the interest of these modalities and their impact on the diagnosis, during and after therapeutic care of brain tumors.

### **Theoretical background. Conventional MRI.**

**The MRI signal origin.** Magnetic resonance imaging is a medical imaging technique used to visualize internal structures of the human body in detail. The MRI makes use of the properties of nuclear magnetic resonance (NMR) to image nuclei of atoms inside the body.<sup>1-5,23</sup> An MRI scanner is equipped with a strong magnet where the magnetic field is used to align the magnetization of water hydrogen nuclei in the body, and radio frequency fields to systematically alter the alignment of this magnetization.<sup>1-5,10,24,25</sup> This causes the nuclei

**Disclosure.** The authors declare no conflicting interests, support or funding from any drug company.

to produce a rotating magnetic field detectable by the MRI scanner coil, and this information is recorded to construct an image of the scanned area of the body.<sup>5,26,27</sup> The magnetic field gradients cause nuclei at different locations to rotate at different speeds. By using gradients in different directions 2D images or 3D volumes can be obtained in any arbitrary orientation. The MRI provides very good contrast between the different soft tissues of the body, which is useful in human tissue imaging, especially the brain.<sup>3,5,10,23-25</sup> The hydrogen proton nuclei of water body tissue become aligned in a large magnetic field.<sup>7</sup> The average magnetic moment of many protons becomes aligned with the direction of the field. A radio frequency transmitter is briefly turned on, producing a varying electromagnetic field. This electromagnetic field has just the right frequency, known as the resonance frequency, to be absorbed and flip the spin of protons in the magnetic field. After the electromagnetic field is turned off, spins of the protons return to thermodynamic equilibrium and the bulk magnetization becomes re-aligned with the static magnetic field. During this relaxation, a radio frequency signal is generated, which can be measured with receiver coils.<sup>5,10,26-37</sup> Information on the origin of the signal in 3D space can be obtained by applying additional magnetic fields during the scan. Protons in different tissues return to their equilibrium state at different relaxation rates. Different tissue variables, including spin density, T1 and T2 relaxation times, and flow and spectral shifts can be used to construct images.<sup>3,5,10-12,23-25</sup> By changing the settings on the scanner, this effect is used to create contrast between different types of body tissue or between other properties, as in diffusion MRI and perfusion MRI. The MRI contrast agents may be injected intravenously to enhance the appearance of blood vessels, tumors, or inflammation.<sup>3,5,10-12,23-25,28</sup>

**T1-weighted MRI.** The T1-weighted scans refer to a set of standard scans that depict differences in the spin-lattice (or T1) relaxation time of various tissues within the body. The T1-weighted contrast can be increased with the application of an inversion recovery RF pulse. The T1-weighted sequences are often collected before and after infusion of T1-shortening MRI contrast agents. In the brain, T1-weighted scans provide appreciable contrast between gray and white matter.<sup>26,29-31</sup>

**T2-weighted MRI.** The T2-weighted scans are another basic type. Like the T1-weighted scan, fat is differentiated from water but in this case fat shows darker, and water lighter. For example, in the case of a cerebral and spinal study, the CSF will be lighter in T2-weighted images. These scans are therefore, particularly well

suited to imaging edema. The T2-weighted images have long been a clinical workhorse.<sup>26,29-31</sup>

**Diffusion imaging.** While the signal attenuation caused by molecular diffusion in the presence of magnetic field gradients was recognized as early as 1954 by Carr and Purcell,<sup>17</sup> the basis of today's diffusion weighted imaging methods were developed by Stejskal and Tanner in 1965.<sup>5</sup> Interest in the potential medical usefulness of the technique was further stimulated by the 1990 discovery by Moseley and co-workers<sup>24</sup> that the apparent diffusion coefficient of cat brain decreased by up to 50% within 30 minutes after the onset of focal ischemia, while the conventional MR images remained normal.<sup>1,15-21,24-27</sup> Molecular diffusion is the result of Brownian motion, the constant random walk of the individual molecules in a fluid due to thermal agitation. Although the mean displacement of the molecules remains zero, as time goes by, there is a non-zero probability of finding an individual molecule at a distance from its point of origin. In fact, the root-mean-square displacement can be shown to increase in proportion to the square root of time, the constant of proportionality being a diffusion constant  $D$  characterizing the fluid studied. At 25°, for instance, the diffusion coefficient of pure water is approximately  $2.2 \times 10^3 \text{ mm}^2/\text{s}$ . Soft tissues tend to behave like aqueous protein solutions and, due to the reduced mobility of the water molecules, the corresponding diffusion coefficient is generally smaller than that of pure water. In many tissues, boundaries with various degrees of permeability hinder the free diffusion of water, further decreasing the diffusion coefficient. Applying the Brownian motion model in these circumstances leads to an 'apparent diffusion coefficient' or ADC, to be distinguished from the diffusion coefficient of free water molecules. In tissues like white brain matter, an additional complication arises from the fact that molecular mobility is not the same in all directions; namely, the diffusion process is anisotropic and the scalar diffusion coefficient must be replaced by a tensor quantity.<sup>7,24,25,27,32-37</sup> Diffusion imaging thus provides a window on the microscopic structures and processes (presence and permeability of membranes, equilibrium intracellular extracellular water, and so forth) inside the tissues as reflected by the motion of the water molecules. In an isotropic environment, molecular mobility can be described by a scalar diffusion coefficient, reflecting the fact that the Brownian motion is similar in all spatial directions. The description of the effect of isotropic diffusion on the spin echo signal is relatively simple in this case. In the absence of magnetic field gradients, the signal is unaffected by the presence of incoherent motion. As soon as field

gradients are switched on during any stage of the signal preparation, the motion leads to spin dephasing that, due to the random nature of the successive trajectories of each individual molecule, cannot be undone. The result is an exponential attenuation of the original signal  $I_0(N(H), T1, T2)$  obtained in the absence of field gradients:

$$I = I_0(N(H), T1, T2) e^{-bD}$$

where  $D$  is the (apparent) diffusion coefficient of the medium and  $b$  is a scalar reflecting the properties of the magnetic field gradient  $G(t)$  driven during the diffusion imaging measurement.<sup>5,7,17,24,25,27,29,33-38</sup>

**Perfusion imaging.** In MR perfusion imaging, the models introduced in the past for nuclear medicine studies remain useful, except that now the tracer is either an intravascular contrast agent or a volume of blood that has been tagged using radio frequency (RF) excitation.<sup>1,12-20,32,36-38</sup> Excellent reviews of the results of kinetic theory that are of interest for MRI have been published in the past,<sup>16,32</sup> and several previous studies include more detailed discussion.<sup>14,16,18,19,34</sup> Moreover, we define additional quantities describing the interaction between blood, tracer, and tissue. The blood-tissue partition coefficient of a tracer expresses the equilibrium distribution of tracer between blood and tissue. For an intravascular tracer, it equals the cerebral blood volume (CBV), while for a freely diffusible tracer it is approximately one. The residue function describes the probability that a molecule of tracer, that entered a voxel at  $t=0$ , is still inside that voxel at a later time  $t$ . It depends on the transport of the tracer between blood and tissue and the subsequent clearance from the tissue volume. Hence, the following assumptions are made in any analysis applying tracer kinetics: 1. The perfusion must be constant and unaffected by the tracer. 2. The tracer must be thoroughly mixed with the blood. 3. The concentration of the tracer can be monitored accurately. 4. Recirculation of the tracer can be corrected for when present.

**Magnetic resonance spectroscopy.** Purcell et al<sup>4</sup> and Bloch et al<sup>1</sup> elucidated the principles of nuclear magnetic resonance in 1946.<sup>2,4,6,8-10,18,22,28,30,37,39-53</sup> Five years later, Proctor and Yu<sup>50</sup> proposed that the resonance frequency of a nucleus depends on its chemical environment, which produces a small, but perceptible, change in the Larmor resonance frequency of that nucleus. This nuclear behavior is termed "chemical shift," and is caused by the magnetic fields generated by circulating electrons surrounding the nuclei interacting with the main magnetic field.<sup>4,8,9,28,30,50,51</sup> Protons ( $^1H$ ) have been traditionally used for MR spectroscopy because of their high natural abundance in organic structures

and high nuclear magnetic sensitivity compared with any other magnetic nuclei.<sup>40,45</sup> Moreover, diagnostically resolvable hydrogen MR spectra may be obtained with clinical instruments (1.5 Tesla or greater) and routine surface coils. Phosphorus  $^{31}P$  MR spectroscopy has also been used clinically to study changes in high-energy metabolism in a number of pathologic processes. However, phosphorus  $^{31}$ , carbon  $^{13}$ , sodium  $^{23}$ , and fluorine  $^{19}$  MR spectroscopy will not be addressed here. Hence, the excitation of hydrogen nuclei exposed to a uniform magnetic field by a RF pulse will rotate them from the equilibrium position. When this pulse is turned off, the hydrogen nuclei return to their equilibrium position. The time it takes them to return to their original equilibrium position is governed by their relaxation times. The receiving coil detects the voltage variations at many points in time during this period. This electric voltage variation is termed free induction decay and may be plotted as an exponential decay function, such as intensity versus time, to yield time domain information, such as relaxation times. Then, the Fourier transformation of this information yields information in the frequency domain; namely, a plot of peaks at different Larmor frequencies. The parameters that characterize each peak include its resonance frequency, its height, and its width at half-height. These MR spectroscopy acquisition steps are similar to the MRI approach. The resonance frequency position of each peak on the plot is dependent on the chemical environment of that nucleus and is usually expressed as parts per million from the main magnetic resonance frequency of the system used (namely, chemical shift). The height (maximum peak intensity) or the area under the peak may be calculated and yield relative measurements of the concentration of protons. The resonance frequency/chemical shift position gives information regarding the chemical environment of protons reflecting the composition of the material studied such as living tissue and tumoral processes. The width of the peak at half-height gives relaxation time information because it is proportional to  $1/T_2$ .<sup>6,11,15,18,22,29,40-45,48-51</sup>

**Positive diagnosis of the brain tumor. Conventional MRI.** The conventional, anatomophysiological, or morphological MRI reports important information mainly concerning the individuality or the multiplicity of the tumoral lesions; the lesion topography expressed in terms of intra-parenchymatous, extra-parenchymatous, or intra-ventricular. The MRI provides precise localization of the tumoral mass and its epicenter allowing better and

direct diagnosis in terms of white matter (argument in favor of astrocytoma) or grey matter (argument in favor of an oligodendroglioma), ependyma (ependymoma, metastasis, lymphoma), nerve (neurinoma), meninx (meningioma, metastasis). The topographical aspect of the tumor: infiltrating or expansive, exophytic or not, curved or polycyclic, with sharp or fuzzy contours, with or without satellite lesion. The extension of a hemispherical lesion within the contralateral hemisphere and also in deeper structures, particularly in the central grey nuclei or brainstem, the tumor volume is also measured in the case of a surgical therapy requirement aiming at full exeresis. The conventional MRI examination does not still allow answering of 5 questions: 1. Is it a tumor? 2. Aggressiveness of the tumor? 3. The delineation of limits of the tumor? 4. The histological classification of the tumor? 5. To differentiate between tumor and radionecrosis?

**Diffusion MRI.** The diffusion MRI study is interesting in miscellaneous diagnostic situations including the imperative differential diagnosis between abscess and tumoral necrosis,<sup>2,8,35,47</sup> as well as between cellular tumors (lymphomas, medulloblastoma, and so forth) and glial malignant tumors metastasis.<sup>10,30,38</sup> The apparent diffusion coefficient (ADC) is an indirect marker of the cellular density.<sup>11</sup> Yamasaki et al<sup>11</sup> demonstrated a negative correlation between the tumoral grade and the ADC values within astrocytoma tumors, the ADC decreased with the increasing tumoral grade. In general, the ADC decreases after hypercellularities.

**Perfusion MRI.** At present, the perfusion MRI is considered a crucial MRI modality in clinical routine for the diagnosis and the therapeutic follow-up of brain tumors by offering access to the cerebral blood volume and thus to the neo-angiogenesis.<sup>19,20,46</sup> The relative cerebral blood volume (rCBV) is obtained using this modality of perfusion MRI (curve of first passage of contrast bolus) that is interesting in the tumoral pathology and is also considered representative of the tumor: the low-grade tumors appear in perfusion MRI with a rCBV lower than 1.5, hence the predictive value allowing exclusion of high-grade tumors.<sup>36</sup> While high-grade tumors mostly demonstrate an rCBV superior to 2 with very high contrast level.<sup>46</sup>

**Magnetic resonance spectroscopy.** The MRS is very sensitive and the most specific technique for the positive diagnosis of brain tumors.<sup>10,22,39,40,41</sup> Compared to healthy brain tissue, the spectra of brain tumors are characterized by: An increase of the choline involved in metabolism, phospholipid membrane structures, choline/creatine (Ch/Cr) and Ch/N-Acetyl-Aspartate

(Ch/NAA) ratios reflecting an altered cell membrane and a cellular proliferation. A decrease of NAA and NAA/Cr showing neuronal loss. Myo-inositol is sugar available only in glia cells; elevated myo-inositol indicates high glial cell activation, especially in cases of low-grade glial tumors. The presence of free lipids is a marker of cellular necrosis; it is related to the brain tumor grade and dominates the spectra in cases of high-grade tumors.

**The differential diagnosis between abscess and brain tumor.** Several papers described diffusion MRI importance in establishing the differential diagnosis between abscess and brain tumoral necrosis.<sup>2,8,35,47</sup> In diffusion MRI, the abscess is discriminated easily in most tumoral necrosis cases. Indeed, considering the high viscosity of the abscess pus, a higher intensity is observed in diffusion MR images opposed to malignant tumor, and the apparent diffusion coefficient (ADC) is explicitly lowered. The ADC value measured in an abscess lesion varies between values of  $0.538 \cdot 10^{-3} \text{ mm}^2/\text{s}^{-1}$  and  $0.67 \pm 0.17 \cdot 10^{-3} \text{ mm}^2/\text{s}^{-1}$ ,<sup>35</sup> and is greatly superior to  $2.73 \pm 0.34 \cdot 10^{-3} \text{ mm}^2/\text{s}^{-1}$  for a tumor.<sup>47</sup>

The contrast bolus course in the abscess wall in perfusion MRI does not correspond to high rCBV. The contrast then is showing the avascular aspect, which is opposed to that observed in necrotic tumor aspects. In the case of abscess, the contrast of T1 images with contrast enhancement is connected to the inflammation process and broken blood brain barrier (BBB) and not to a neovascularization. In MR spectroscopy, revealed multiple amino acids result from the degradation of polynuclear neutrophils synthesized by bacteria. The peak of the spectrum is centered on 0.9 ppm confirming the positive diagnosis of progenia of untreated abscess.<sup>2,12,18,42,48</sup> While the presence of acetate and succinate peaks is expressing the bacterial metabolism associated with a lactate peak (Figure 1).

**Brain tumor assessment. Low-grade glioma.** Low-grade glioma is an infiltrating lesion appearing with low intensity in T1 images with high intensity in T2/FLAIR MR images and without contrast enhancement. Low-grade glioma demonstrates low signal intensity in diffusion MRI associating a high ADC value. In addition, glioma demonstrates perfusion MRI with an rCBV lower than 1.5, which is an exclusive predictive value of high-grade tumors.<sup>36</sup> These aspects are translated in MRS with higher myo-inositol, a moderate increase of Ch, Ch/Cr, and Ch/NAA ratios with the absence of free lipids. The detection of lactate within the tumoral lesion translates an underlying development process;<sup>44</sup> its production translates an acceleration of anaerobic glycolysis (Figure 2).

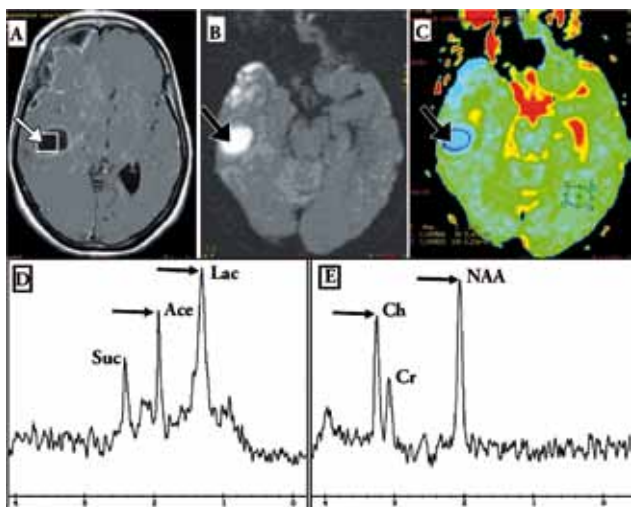


**Figure 1** - Multimodal MRI of abscess showing A) the axial T1 image after bolus injection demonstrated annular enhancement, the white square demonstrates the localization studied by MR spectroscopy. The diffusion image demonstrated an important increase of the signal in the lesion reflection diffusion restriction B); while the apparent diffusion coefficient (map demonstrated a clear decrease of the signal in the lesion C). The monovoxel MRS with short echo time demonstrated the presence of an important quantity of lactate (Lac) and acetate (Ace) markers of infection and succinate (Suc) metabolites found in most brain abscesses D); while the monovoxel MRS with long echo times E) demonstrated a Ch/NAA ratio less than one that discarding the tumoral character of the lesion. Ch - choline, NAA - N-Acetyl-Aspartate, Cr - creatine

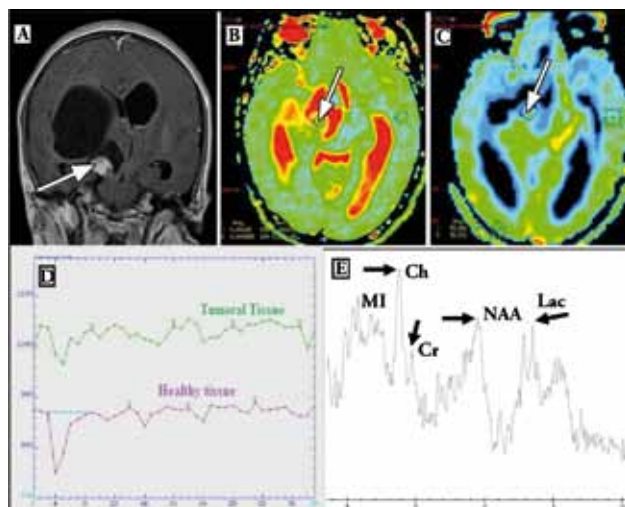


**Figure 2** - Multimodal MRI of a low grade tumor (pilocytic astrocytoma) demonstrated a contrast enhancement reflecting the blood brain barrier rupture A); while the apparent diffusion coefficient (ADC) map demonstrated a moderate increase of ADC value B). The perfusion maps and the perfusion relative cerebral blood volume (rCBV) curve of both healthy and tissue lesion C) and D) did not demonstrate any increased of the rCBV. The MR spectroscopy with short echo time demonstrated a moderate increase of the Ch/Cr and Ch/NAA ratios and presence myo-inositol (MI) and lactate E). Ch - choline, Cr - creatine, NAA - N-Acetyl-Aspartate

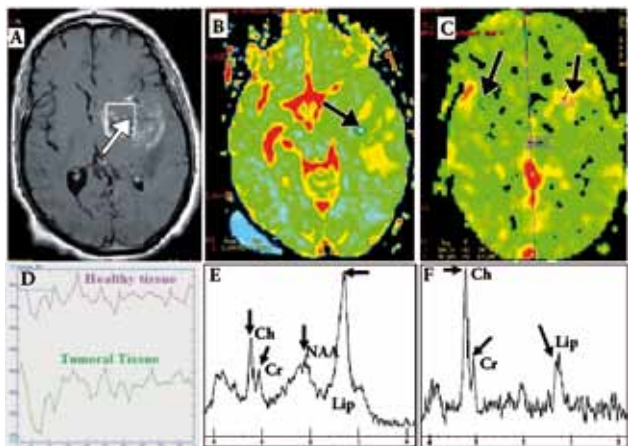


**Figure 3** - Multimodal MRI of a glioblastoma in axial T1 image after paramagnetic bolus injection A), the white square corresponds to the localization studied with MR voxel spectroscopy. The apparent diffusion coefficient (ADC) map demonstrated a decreased ADC value in the lesion b). The perfusion maps and the perfusion relative cerebral blood volume (rCBV) curve of both lesion and healthy tissues demonstrated an increased rCBV in the lesion expressing the higher vascularization of the tumor C) and D); while the MRS of short and long echo times E) and F) demonstrated a massive presence of free lipids (Lip) associating a remarkable increase of the Ch/Cr and Ch/NAA ratios. Ch - choline, Cr - creatine, NAA - N-Acetyl-Aspartate

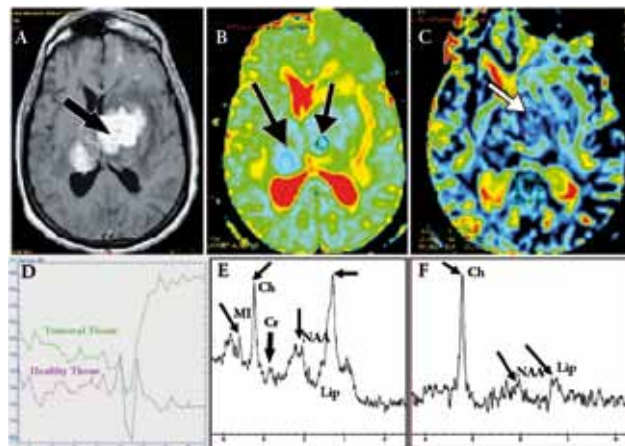


**Figure 4** - Multimodal MRI of lymphoma demonstrated a deep multiple hemispherical intra-parenchymatous lesion with signal enhancement of T1 MR images in the lesion after bolus injection A). The apparent diffusion coefficient (ADC) map demonstrated a decreased diffusion in the lesion B); while the perfusion MRI demonstrated a slightly reduced relative cerebral blood volume (rCBV) in the lesion compared to healthy tissue C) and D). The monovoxel MRS with short echo time demonstrated a high quantity of lipids (Lip) and moderate rise of myo-inositol (MI) E); while the monovoxel MRS with long echo time demonstrated a significant increase of the choline (Ch) and an important decrease of NAA and the creatine (Cr) with presence of a residual lipids peak F). NAA - N-Acetyl-Aspartate

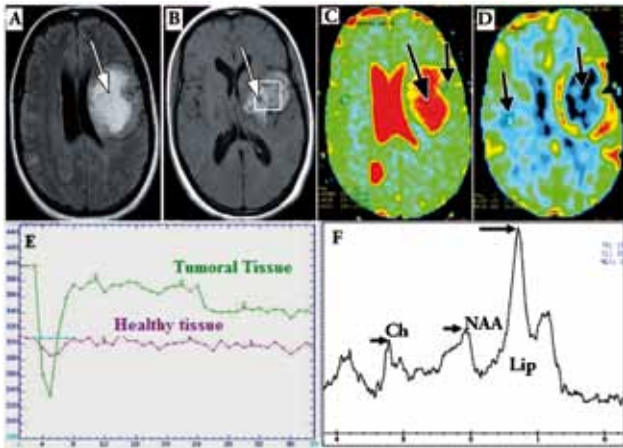


**Figure 5** - Multimodal MRI demonstrated metastasis in FLAIR image A) and T1 with contrast enhancement B), the white square demonstrates the localization studied by MR spectroscopy. The apparent diffusion coefficient (ADC) map demonstrates a slight increase of the ADC value within the lesion C); while the perfusion map and the relative cerebral blood volume (rCBV) perfusion curve of both healthy and lesion tissues D) and E) demonstrated a highly decreased rCBV reflecting the high vascularization of the tumor. The MRS with short echo time demonstrated a massive quantity of free lipids (Lip) associating a global decrease of metabolites confirming the necrotic character of the lesion F). Ch - choline, NAA - N-Acetyl-Aspartate

**High-grade glioma.** High-grade glioma is a heterogeneous lesion demonstrating a contrast enhancement surrounding edema. They demonstrate an iso-signal in diffusion images with a decreased ADC value that is negatively correlated with the tumoral grade.<sup>11</sup> In most cases, high-grade glioma demonstrates an rCBV between 2 and 5 in perfusion MRI with contrast enhancement.<sup>39</sup> In MRS the high-grade glioma are characterized by an important rise of the choline peak that is linearly correlated with the histological proliferation index Ki67,<sup>51</sup> a decreased creatine and NAA peak, a decrease or even a disappearance of the myo-inositol, and presence of free lipids expressing the cellular necrosis, which increases with tumoral grade. Consequently, remote spectra contrast enhancement remains abnormal, with low free lipids reflecting the infiltration (Figure 3).

**Lymphoma.** The lymphoma is an extremely cellular tumor characterized by a high density of confined mass or with a diffuse infiltration and periventricular. It demonstrates a high signal in T1 and intermediate signal in T2/FLAIR MR images. It is surrounded by edema; in addition, it is and frankly and homogeneously contrast enhanced because of the broken BBB. The lymphoma demonstrates a higher signal in diffusion MRI with a low ADC value reflecting the hyper-cellular character of the tumor. The perfusion imaging demonstrates

often normal and even decreased rCBV.<sup>37</sup> In MRS, the lymphoma shows an increase of Ch, a significant decrease of the peaks of NAA and Cr, and clear rise of free lipids, which persists even on the remote spectra of the contrast (Figure 4).

**Metastases.** The brain metastases are contrast enhanced in annular or nodular mode and generally surrounded by edema, and show high ADC values. Metastases and especially hypervascular metastases demonstrate high rCBV in perfusion MRI. In MRS, metastases are expressed by an abundance of free lipids, a moderate rise of the Ch peak, and very low even disappearance of NAA and Cr (Figure 5). The remote spectra with contrast enhancement demonstrates a normal aspect testifying to the non-infiltrating character of these tumor types.<sup>32</sup>

**The extended local assessment of malignant glioma.** In conventional MRI, the glial malignant tumor shows aspects of a necrotic-cystic lesion with strong contrast bolus enhancement surrounded by high signal in T2 and FLAIR images. This aspect could correspond either to a vasogenic shock edema or a tumoral infiltration. The MRS is efficient and allows differentiating between these 2 lesion profiles; it demonstrates specifically the pure edema and tumoral infiltration.<sup>52</sup> The spectra remains normal in vasogenic shock edema, while in a tumoral infiltration spectra appears abnormal and characterized by a rise of Cho/Cr and Cho/NAA ratios.

**Therapeutical follow-up. Pre-therapeutical evaluation.** The diffusion MRI associated with perfusion MRI and MR spectroscopy, allows defining more accurately the potential targets of stereotaxic biopsy and radiotherapy, including the tumor presenting lowered ADC, hyper vascularization and an important increase of choline while it does not correspond necessarily to the intensity level of the contrast enhancement in T1 MR images.<sup>49</sup> The precise demarcation of the tumoral lesion limits allows facilitating to specify the required surgical exeresis such as total or subtotal whenever surgery of the lesion is possible.<sup>29</sup> In order to determine the functional brain areas close to the lesion targeted by the therapist, the functional MRI is required. It allows visualization of the motor, language, and memory areas, and better guidance of the lesion delineation.

**Therapeutical follow-up.** Generally, it is difficult to differentiate early stage tumor and radionecrosis on conventional MRI. The comparison of various MRI modalities provides important results in this regard; the persistence or the evolvement of the lesion is expressed in MRS by a rise of choline, whereas a radionecrosis is translated by a spectra where all metabolites disappear except free lipids.<sup>36</sup> The radionecrosis is not associated

with a neoangiogenesis, but with a vascular necrosis with an rCBV inferior to one; while an rCBV upper to 2.6 is directing to recurrent lesion.<sup>45</sup> Therefore, an early increase of ADC after treatment allows prediction of a decrease of the cellular constituents and would translate a satisfactory therapeutic answer.

In conclusion, a multimodal MRI approach plays an important role in the exploration strategies and care of brain tumors. This imaging approach allows better therapy targeting, including the neurosurgery techniques to be used. The MRS spectroscopy has been shown to be a very sensitive diagnostic and follow-up technique for brain tumors; however, not very specific. Indeed, a better combination of anatomophysiological, functional studies including diffusion tensor MRI, perfusion MRI, BOLD activation, and metabolic localized MRS and MRS imaging, with the support of advanced technological developments, multichannel coils, magnets, and efficient computing software, would allow an improvement in the preciseness of the answers to therapy questions before, during, or after the treatment of brain lesions.

## References

- Bloch R, Hansen WW, Packard M. Nuclear induction. *Phys Rev* 1946; 70: 460-474.
- Ebisu T, Tanaka C, Umeda M, Kitamura M, Naruse S, Higuchi T, et al. Discrimination of brain abscess from necrotic or cystic tumors by diffusion-weighted echo planar imaging. *Magn Reson Imaging* 1996; 14: 1113-1116.
- Lauterbur PC. Image Formation by Induced Local Interactions: Examples of Employing Nuclear Magnetic Resonance. *Nature* 1973; 242: 190-191.
- Purcell EM, Torrey HC, Pound RV. Resonance absorption by nuclear magnetic moments in solids. *Phys Rev* 1946; 69: 37-38.
- Stejskal EO, Tanner JE. Spin diffusion measurements: spin echoes in the presence of a time-dependent field gradient. *J Chem Phys* 1965; 42: 288-292.
- Galanaud D, Chinot O, Metellus P, Cozzone P. Magnetic resonance spectroscopy in gliomas. *Bull Cancer* 2005; 92: 327-331.
- Luechinger R, Duru F, Candinas R, Boesiger P. Safety considerations for magnetic resonance imaging of pacemaker and ICD patients. *Herzschrittmachertherapie und Elektrophysiologie* 2004; 15: 73-81.
- Remy C, Grand S, Lai ES, Belle V, Hoffmann D, Berger F, et al. 1H MRS of human brain abscesses in vivo and in vitro. *Magn Reson Med* 1995; 34: 508-514.
- Sanders JA, Orrison WW. Functional magnetic resonance imaging. In: Orrison WW, Lewine JD, Sanders JA, Hartshorne MF, editors. *Functional Brain Imaging*. St Louis (MO): Mosby; 1995. p. 145-326.
- Vion-Dury J, Salvan AM, Cozzone PJ. Proton magnetic resonance spectrometry for the non-invasive exploration of human brain metabolism: current and future clinical applications. *Rev Neurol* 1999; 155: 903-926.
- Yamasaki F, Kurisu K, Satoh K, Arita K, Sugiyama K, Ohtaki M. Apparent diffusion coefficient of human brain tumors at MR imaging. *Radiology* 2005; 235: 985-991.
- Zierler KL. Theoretical basis of indicator-dilution methods for measuring flow and volume. *Circ Res* 1962; 10: 393-407.
- Counter SA, Olofsson A, Borg E, Bjelke B, Häggström A, Grahn HF. Analysis of magnetic resonance imaging acoustic noise generated by a 4.7 T experimental system. *Acta Otolaryngol* 2000; 120: 739-743.
- Awasthi R, Verma SK, Haris M, Singh A, Behari S, Jaiswal AK, et al. Comparative evaluation of dynamic contrast-enhanced perfusion with diffusion tensor imaging metrics in assessment of corticospinal tract infiltration in malignant glioma. *J Comput Assist Tomogr* 2010; 34: 82-88.
- Bottomley PA, Foster TB, Darrow RD. Depth-resolved surface-coil spectroscopy (DRESS) for in Vivo 1H, 31P, and 13C NMR. *J Magn Reson* 1984; 59: 338-342.
- Buxton RB, Frank LR, Prasad PV. Principles of diffusion and perfusion MRI. In: Edelman RR, Hesselinck JR, Zlatkin MB, editors. *Clinical magnetic resonance imaging*. 2nd ed. Philadelphia (PA): WB Saunders; 1996. p. 233-270.
- Carr HY, Purcell EM. Effects of diffusion on free precession in nuclear magnetic resonance experiments. *Phys Rev* 1954; 94: 630-638.
- Chiang IC, Hsieh TJ, Chiu ML, Liu GC, Kuo YT, Lin WC. Distinction between pyogenic brain abscess and necrotic brain tumour using 3-tesla MR spectroscopy, diffusion and perfusion imaging. *Br J Radiol* 2009; 82: 813-820.
- Chu JP, Mak HK, Yau KK, Zhang L, Tsang J, Chan Q, et al. Pilot study on evaluation of any correlation between MR perfusion (Ktrans) and diffusion (apparent diffusion coefficient) parameters in brain tumors at 3 Tesla. *Cancer Imaging* 2012; 23; 12: 1-6.
- Cotton F, Ongolo-Zogo P, Louis-Tisserand G, Streichenberger N, Hermier M, Jouvret A, et al. [Diffusion and perfusion MR imaging in cerebral lymphomas]. *J Neuroradiol* 2006; 33: 220-228. French
- Damadian R. Tumor detection by nuclear magnetic resonance. *Science* 1971; 171: 1151-1153.
- De Edelenyi FS, Rubin C, Estève F, Grand S, Décorps M, Lefournier V, et al. A new approach for analyzing proton magnetic resonance spectroscopic images of brain tumors: nosologic images. *Nat Med* 2000; 6: 1287-1289.
- Lauterbur PC. Magnetic resonance zeugmatography. *Pure and Applied Chemistry* 1947; 40: 149-157.
- Moseley ME, Cohen Y, Mintorovitch J, Chileuit L, Shimizu H, Kucharczyk J, et al. Early detection of regional cerebral ischemia in cats: comparison of diffusion- and T2-weighted MRI and spectroscopy. *Magn Reson Med* 1990; 14: 330-346.
- Moseley ME, Cohen Y, Kucharczyk J. Diffusion-weighted MR imaging of anisotropic water diffusion in cat central nervous system. *Radiology* 1990; 176: 439-445.
- Squire LF, Novelline RA. *Squire's fundamentals of radiology*. 5th ed. Cambridge (MA), London (UK): Harvard University Press; 1997.
- Luytpaert R, Boujraf S, Sourbron S, Osteaux M. Diffusion and perfusion MRI: basic physics. *Eur J Radiol* 2001; 38: 19-27.
- Qian X, Wei L. The VDS based Compressed Sensing for abdomen MRI. *Advances in Computational Mathematics and its Applications (ACMA)* 2012; 1: 12-16.

29. Nelson SJ, Graves E, Pirzkall A, Li X, Antiniw Chan A, Vigneron DB, et al. In vivo molecular imaging for planning radiation therapy of gliomas: an application of 1H MRSI. *J Magn Reson Imaging* 2002; 16: 464-476.
30. Rees J. Advances in magnetic resonance imaging of brain tumours. *Curr Opin Neurol* 2003; 16: 643-650.
31. Sheil WC. Magnetic Resonance Imaging (MRI Scan). MedicineNet 2012 [updated 2007 May 3; cited 2012 April 27] Available from: [http://www.medicinenet.com/mri\\_scan/article.htm](http://www.medicinenet.com/mri_scan/article.htm)
32. Law M, Cha S, Knopp EA, Johnson G, Arnett J, Litt AW. High-grade gliomas and solitary metastases: differentiation by using perfusion and proton spectroscopic MR imaging. *Radiology* 2002; 222: 715-721.
33. Le Bihan D. Molecular diffusion nuclear magnetic resonance imaging. *Magn Reson Q* 1991; 7: 1-30.
34. Le Bihan D, Breton E, Lallemand D, Grenier P, Cabanis E, Laval-Jeantet M. MR imaging of intravoxel incoherent motions: application to diffusion and perfusion in neurologic disorders. *Radiology* 1986; 161: 401-407.
35. Leuthardt EC, Wippold FJ 2nd, Oswood MC, Rich KM. Diffusion-weighted MR imaging in the preoperative assessment of brain abscesses. *Surg Neurol* 2002; 58: 395-402.
36. Lev MH, Ozsunar Y, Henson JW, Rasheed AA, Barest GD, Harsh GR 4th, et al. Glial tumor grading and outcome prediction using dynamic spin-echo MR susceptibility mapping compared with conventional contrast-enhanced MR: confounding effect of elevated rCBV of oligodendrogliomas. *AJNR Am J Neuroradiol* 2004; 25: 214-221.
37. Faehndrich J, Weidauer S, Pilatus U, Oszvald A, Zanella FE, Hattingen E, et al. Neuroradiological viewpoint on the diagnostics of space-occupying brain lesions. *Clin Neuroradiol* 2011; 21: 123-139.
38. Martin-Duverneuil N, Guillevin R, Chiras J. Imaging of gliomas. *Cancer Radiother* 2008; 12: 669-675.
39. Filler AG. The history, development, and impact of computed imaging in neurological diagnosis and neurosurgery: CT, MRI, DTL. *The Internet Journal of Neurosurgery* 2010; 7: 1.
40. Galanaud D, Chinot O, Nicoli F, Confort-Gouny S, Le Fur Y, Barrie-Attarian M, et al. Use of proton magnetic resonance spectroscopy of the brain to differentiate gliomatosis cerebri from low-grade glioma. *J Neurosurg* 2003; 98: 269-276.
41. Galanaud D, Nicoli F, Figarella-Branger D, Roche P, Confort-Gouny S, Le Fur Y, et al. [MR spectroscopy of brain tumors]. *J Radiol* 2006; 87: 822-832. French.
42. Grand S, Ternier J, Rousseau N, Ashraf A, Tropres I, Remy C, et al. Cerebral abscess: MRI, DWI and MRS features. *J Neuroradiol* 2004; 31: 145-147.
43. Grand S, Tropres I, Hoffmann D, Ziegler A, Le Bas JF. Proton magnetic resonance spectroscopy (1H-MRS) for the diagnosis of brain tumors and the evaluation of treatment. *Neurochirurgie* 2005; 51: 299-308.
44. Guillevin R, Menuel C, Duffau H, Kujas M, Capelle L, Aubert A, et al. Proton magnetic resonance spectroscopy predicts proliferative activity in diffuse low-grade gliomas. *J Neurooncol* 2008; 87: 181-187.
45. Kimura T, Sako K, Gotoh T, Tanaka K, Tanaka T. In vivo single-voxel proton MR spectroscopy in brain lesions with ring-like enhancement. *NMR Biomed* 2001; 14: 339-349.
46. Kremer S, Grand S, Remy C, Esteve F, Lefournier V, Pasquier B, Hoffmann D, et al. Cerebral blood volume mapping by MR imaging in the initial evaluation of brain tumors. *J Neuroradiol* 2002; 29: 105-113.
47. Lai PH, Ho JT, Chen WL, Hsu SS, Wang JS, Pan HB et al. Brain abscess and necrotic brain tumor: discrimination with proton MR spectroscopy and diffusion-weighted imaging. *AJNR Am J Neuroradiol* 2002; 23: 1369-1377.
48. Lai PH, Hsu SS, Ding SW, Ko CW, Fu JH, Weng MJ, et al. Proton magnetic resonance spectroscopy and diffusion-weighted imaging in intracranial cystic mass lesions. *Surg Neurol* 2007; 68 Suppl 1: S25-S36.
49. Laprie A. Proton magnetic resonance spectroscopic imaging and other types of metabolic imaging for radiotherapy planning in adult and pediatric high-grade gliomas. *Cancer Radiother* 2009; 13: 556-561.
50. Protor WG, Yu FC. The dependence of nuclear magnetic resonance frequency upon chemical shift. *Physiol Rev* 1950; 70: 717.
51. Schimitzu H, Kumabe T, Shirane R, Yoshimoto T. Correlation between choline level measured by proton MR spectroscopy and Ki-67 labeling index in gliomas. *AJNR Am J Neuroradiol* 2000; 21: 659-665.
52. Pierot L. Neuroradiology. *J Radiol* 2005; 86: 868-873.
53. Stadnik TW, Chaskis C, Michotte A, Shabana WM, Van Rompacy K, Luypaert R, et al. Diffusion-weighted MR imaging of intracerebral masses: comparison with conventional MR imaging and histologic findings. *AJNR Am J Neuroradiol* 2001; 22: 969-976.

## COPYRIGHT

Whenever a manuscript contains material (tables, figures, etc.) which is protected by copyright (previously published), it is the obligation of the author to obtain written permission from the holder of the copyright (usually the publisher) to reproduce the material in Neurosciences. This also applies if the material is the authors own work. Please submit copies of the material from the source in which it was first published.